Supporting Information

Electrostatic consideration of ZnO crystal.

As shown in Fig. S1(a), the ZnO crystal with a hexagonal rod shape elongated along the *c*-axis is conventionally achieved due to a large anisotropic growth habit of the individual facet, $V_{[0001]} >> V_{[01\text{-}10]} > V_{[000\text{-}1]}$.[1, 2] As a consequence of such a typical growth habit, two different polar surfaces as the Zn-(0001) plane and O-(000-1) one are naturally created on opposite direction of the ZnO crystal. According to the classical electrostatics, however, this ionic crystal with alternating layers of opposite charge density (marked $\pm \sigma$ in Fig. S1(b)) induces highly unstable situation because a net dipole moment and electrostatic potential increase monotonically upon increasing slab thickness along the *c*-axis as shown in Fig. S1(c).[3-5] In order to overcome such a instability of the ideal ionic crystal, a rearrangement of the surface charge density between the Zn-(0001) and O-(000-1) should be developed by a factor of $\sigma' = \sigma R_2/(R_1 + R_2) \approx 0.76\sigma$, where R_1 and R_2 are interlayer spacing between Zn^{2+} and O^{2-} ions as represented in Fig. S1(b), through an effective charge transfer of 0.17electrons from the O-(000-1) plane to the Zn-(0001) one.[4, 6] Consequently, the O-(000-1) surface (or the Zn-(0001) one) is less negative (or positive) and the monotonic increase of the electronic potential in the ZnO crystal could be also suppressed as shown in Fig. S1(d).[3]

Temperature resolved XRD study of Zn-HDS-60h.

Temperature resolved XRD patterns were obtained by heating from room-temperature (RT) to 150˚C in the conventional furnace. Fig. S2(a) shows the XRD pattern of the Zn-HDS-60h with interlayer spacing of 20.0 Å and the (00*l*) peaks were shifted toward high angle, which the new (00*l*) peaks are corresponding to the interlayer spacing of 16.0 Å, by heating at 50 and 100 °C as shown in Fig. S2(b) and (c). Fig. S2(d) shows the interlayer distance of the Zn-HDS-60h is completely changed from 20.0 Å to 16.0 Å by heating at 150°C. This result implies that water molecules were intercalated as double layer into the Zn-HDS-60h. In usually, eliminating temperature of the interlayer water is higher than the normal boiling temperature (100 °C) due to protection from the external thermal energy by the inorganic unit blocks. One of the interesting facts is that such a decrease of the interlayer distance was immediately recovered from 16.0 Å to 20.0 Å under the ambient humidity condition for a few hours. It demonstrates that the water molecules in the Zn-HDS-60h play important role in the electrostatic charge compensation between the intercalated molecules and building blocks.

Inductively coupled plasma (ICP) and elemental (CHN) analysis of Zn-HDS-1h and Zn-HDS-60h.

From inductively coupled plasma (ICP) analysis, Zn concentration in 10 mg weight of the Zn-HDS-1h and the Zn-HDS-60h was determined as 8.10×10^{-5} mol and 8.26×10^{-5} mol, respectively. In addition, Wt% of C, H, and N elements in 10mg was 7.8% (C), 2.9% (H), 0.0% (N) for the Zn-HDS-1h and 4.9% (C), 3.0% (H), 0.0% (N) for the Zn-HDS-60h. The general formula of HDSs is $[(M^{2+}_{1-x}, M'^{2+}_{1+x})(OH)_{3(1-y)}]^{+}X^{n-}_{(1+3y)/n}\cdot zH_2O$ in which M and M′ corresponds to divalent transition metals (Cu, Co, Ni, Mn, and Zn) and X^{n-} is the intercalated anions.[8] In the present study, M and M′ is Zn and X is CH_3COO^{-} for the Zn-HDS-1h and CH_3COO^{-} and CO_3^{2-} for the Zn-HDS-60h as well explained by FT-IR study. Therefore, formula of the Zn-HDS-1h and the Zn-HDS-6h could be represented as $[Zn_2(OH)_{3(1-y)}]^{+}CH_3COO^{-}_{(1+3y)}\cdot zH_2O$ and $[Zn_2(OH)_{3(1-y)}]^{+}[CH_3COO]^{-}_{(1+3y)}[CO_3]^{2-}_{(1+3y)/2}\cdot zH_2O$, respectively. From the ICP and CHN analysis, the y parameter was determined as -0.067 for the Zn-HDS-1h and -0.198 for the Zn-HDS-60h and the z parameter corresponds to 0.8 for the Zn-HDS-1h and 1.2 for the Zn-HDS-60h. Therefore, composition stoichiometry of the Zn-HDS-1h and Zn-HDS-60h is $Zn_2(OH)_{3.2}(CH_3CO_2^-)_{0.8}\cdot 0.8H_2O$ and $Zn_2(OH)_{3.6}(CH_3CO_2^-)_{0.4}(CO_3^{2-})_{0.2}\cdot 1.2H_2O$, respectively.

References.

1. J. -H. Choy, E. -S. Jang, J. -H. Won, J. H. Chung, D. J. Jang and Y. W. Kim, *Adv. Mater.*, 2003, **15**, 1911.

2. J. -H. Choy, E. -S. Jang, J. -H. Won, J. H. Chung, D. J. Jang and Y. W. Kim, *Appl. Phys. Lett.,* 2004, **84**, 287.

3. C. Noguera, *J. Phys.: Condens. Matter,* 2000, **12**, R367.

4. O. Dulub, U. Diebold and G. Kresse, *Phys. Rev. Lett.*, 2003, **90**, 016102.

5. B. Meyer and D. Marx, *Phys. Rev. B*, 2003, **67**, 035403.

6. A. Wander, F. Schendin, P. Steadman, A. Norris, R. McGrath, T. S. Turner, G. Thornton and N. M. Harrison, *Phys. Rev. Lett.*, 2001, **86**, 3811.

7. K. Nakamoto, Infrared and Raman Spectra of Inorganic and Coordination Compounds, Part B: Applications in Coordination, Organometallic, and Bioinorganic Chemistry, 5th ed., *Wiley-Interscience*, New York, 1997.

8. L. Poul, N. Jouini and F. Fiévet, *Chem. Mater.*, 2000, **12**, 3123.

Figure captions.

Fig. S1. (a) Crystal structure of the hexagonal ZnO rod. (b) Charge distribution in ZnO crystal along the *c*-axis. R1 and R2 are interlayer spacing between Zn^{2+} and O^{2-} and $\pm\sigma$ is charge density of alternative layers along the normal to the surface. (c) and (d) Variation of electric field (E) and potential (V) upon the number (*N*) of double layer with opposite charge along the *c*-axis (adapted from Ref. 3).

Fig. S2. Temperature resolved XRD patterns of the Zn-HDS-60h obtained from heat treatment at (c) RT, (b) 50, (c) 100, and (d) 150 °C.

Table S1. Infrared frequencies and band assignments for acetate and carbonate molecules intercalated into the interlayer of Zn-HDS (adapted from Ref. 7).

Table S2. Correlation table for D_{3h}, C_{2v}, and C_s (adapted from Ref. 7).

Fig. S1.

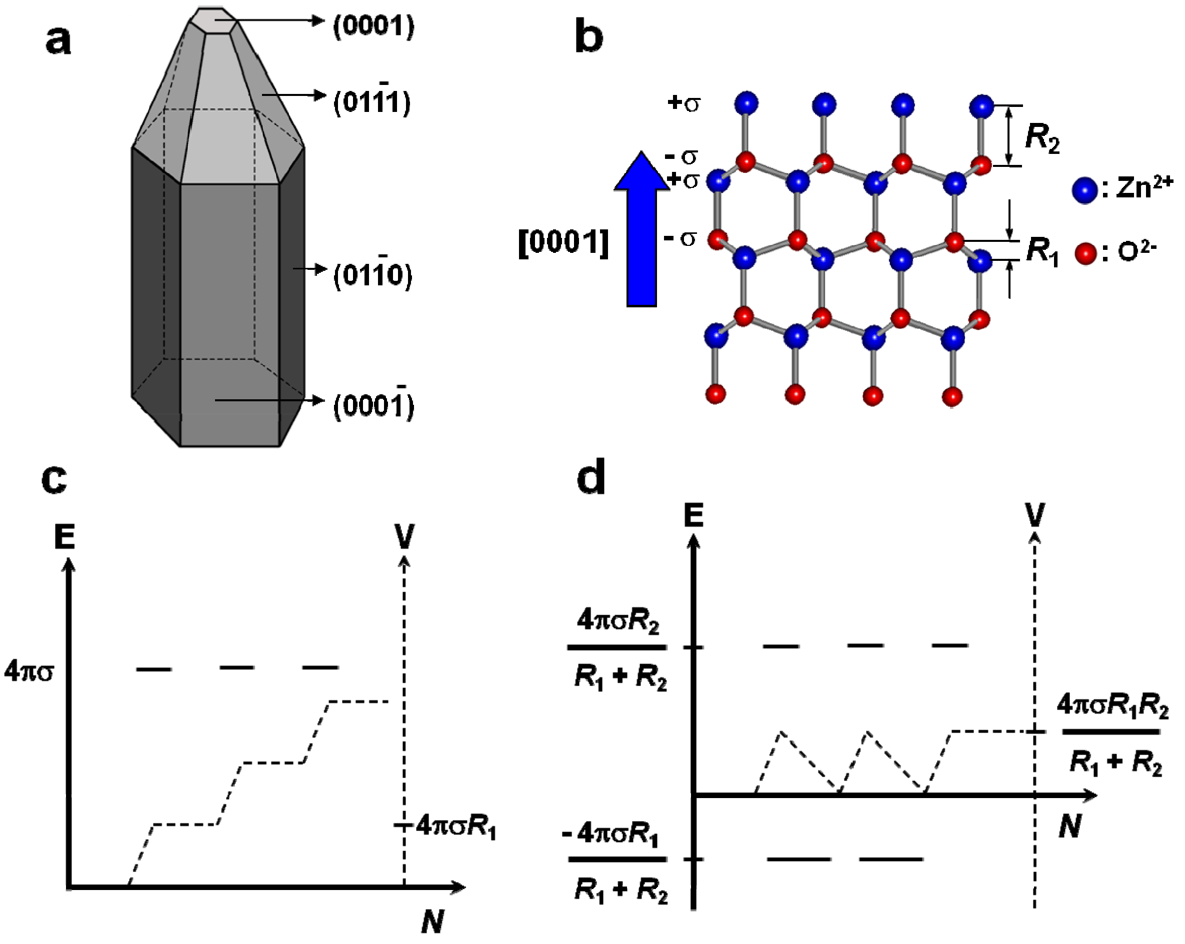
a
(0001)
$(01\bar{1}1)$
$(01\bar{1}0)$
$(000\bar{1})$
b
$+\sigma$
$-\sigma$
$+\sigma$
$-\sigma$
[0001]
R_2
R_1
: Zn^{2+}
: O^{2-}
c
E
V
$4\pi\sigma$
$4\pi\sigma R_1$
N
d
E
V
$\frac{4\pi\sigma R_2}{R_1 + R_2}$
$\frac{4\pi\sigma R_1 R_2}{R_1 + R_2}$
$\frac{-4\pi\sigma R_1}{R_1 + R_2}$
N

Fig. S2.

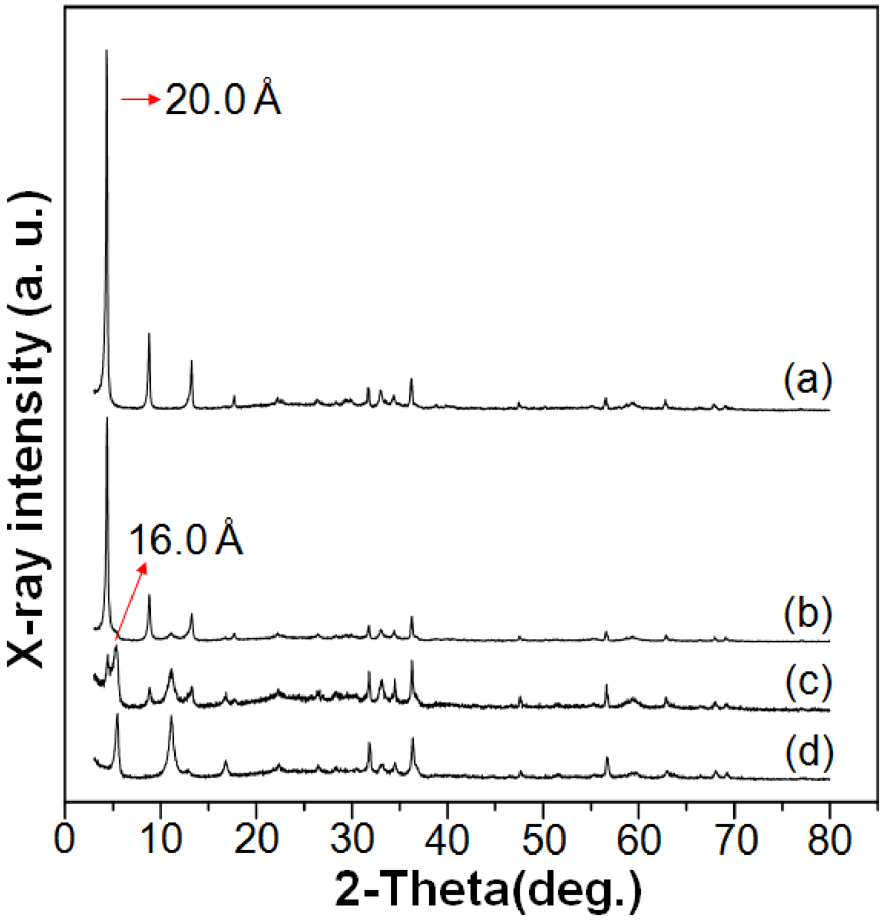
20.0 Å
16.0 Å
(a)
(b)
(c)
(d)
X-ray intensity (a. u.)
2-Theta(deg.)
0
10
20
30
40
50
60
70
80

Table S1.

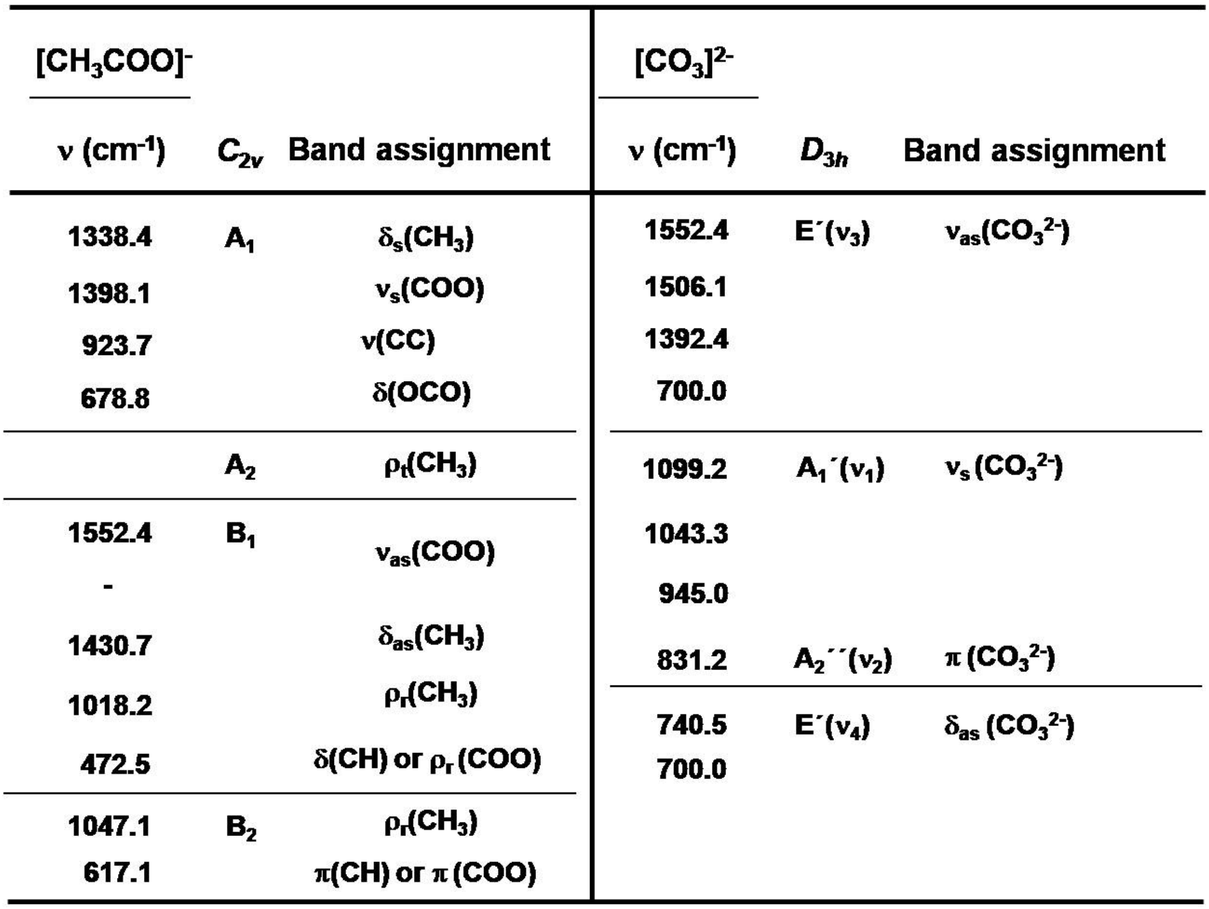

$[CH_3COO]^-$			$[CO_3]^{2-}$		
ν (cm^{-1})	C_{2v}	Band assignment	ν (cm^{-1})	D_{3h}	Band assignment
1338.4	A_1	$\delta_s(CH_3)$	1552.4	$E'(\nu_3)$	$\nu_{as}(CO_3^{2-})$
1398.1		$\nu_s(COO)$	1506.1		
923.7		$\nu(CC)$	1392.4		
678.8		$\delta(OCO)$	700.0		
	A_2	$\rho_t(CH_3)$	1099.2	$A_1'(\nu_1)$	$\nu_s(CO_3^{2-})$
1552.4	B_1	$\nu_{as}(COO)$	1043.3		
-			945.0		
1430.7		$\delta_{as}(CH_3)$	831.2	$A_2''(\nu_2)$	$\pi(CO_3^{2-})$
1018.2		$\rho_r(CH_3)$	740.5	$E'(\nu_4)$	$\delta_{as}(CO_3^{2-})$
472.5		$\delta(CH)$ or $\rho_r(COO)$	700.0		
1047.1	B_2	$\rho_r(CH_3)$			
617.1		$\pi(CH)$ or $\pi(COO)$			

ν; stretching, δ; in-plane bending, ρ_r; rocking, ρ_t; twisting, π; out-of-plane bending. Subscripts *as* and *s* denote antisymmetric and symmetric modes, respectively.

Table S2.

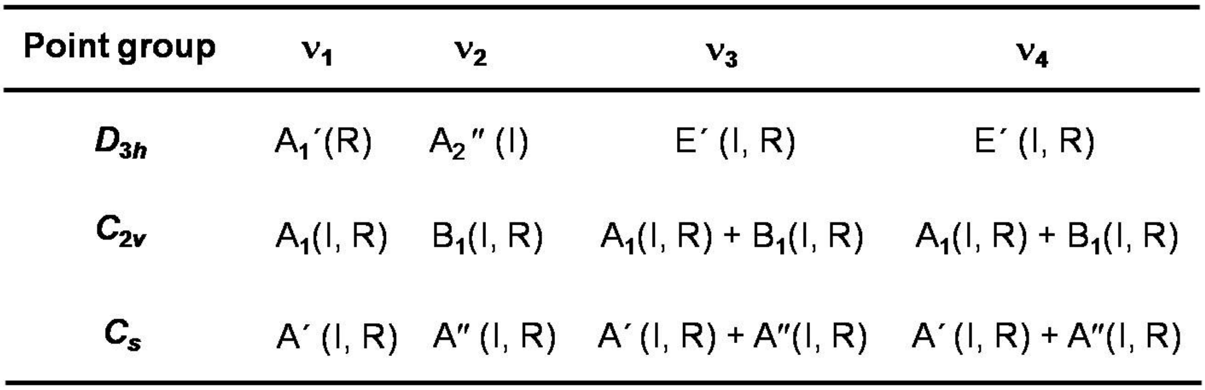

Point group	ν_1	ν_2	ν_3	ν_4
D_{3h}	A_1'(R)	A_2'' (I)	E′ (I, R)	E′ (I, R)
C_{2v}	A_1(I, R)	B_1(I, R)	A_1(I, R) + B_1(I, R)	A_1(I, R) + B_1(I, R)
C_s	A′ (I, R)	A″ (I, R)	A′ (I, R) + A″(I, R)	A′ (I, R) + A″(I, R)